Sustainable Cities and Society 50 (2019) 101671

Contents lists available at ScienceDirect

Sustainable Cities and Society

journal homepage: www.elsevier.com/locate/scs

Assessment of urban human mobility perturbation under extreme weather events: A case study in Nanjing, China

Fucheng Zhang, Zaishang Li, Nan Li*, Dongping Fang

Department of Construction Management, Tsinghua University, Beijing, 100084, China

ARTICLE INFO

Keywords:
Extreme weather event
Human mobility
Perturbation
Assessment
Trajectory
Case study

ABSTRACT

Extreme weather events (EWEs), due to their high uncertainty, massive scale, irreversibility and destructiveness, may significantly impact cities, including causing notable perturbation to urban human mobility. Recent research has substantially advanced the knowledge on general human mobility patterns in cities, primarily about the spatiotemporal characteristics of trajectories of urban population, but has rarely examined the perturbation of these mobility patterns during EWEs. To quantitatively assess human mobility perturbation, this study proposes to measure both the instantaneous perturbation at any given moment during an EWE, and the accumulated perturbation over the entire timespan of the EWE. Using two metrics that are developed for the above purpose, a case study is conducted in Nanjing, a major city in China, which recently experienced record-breaking rainstorm and snowstorm events. Based on trajectories of all taxies and buses in Nanjing during these events, the case study quantitatively assesses the perturbation of human mobility in the city, compares it between two EWEs and between two modes of transport, and analyzes the geographical distribution of the perturbation within the city boundary. Based on the results, further insights into the impacts of EWEs on urban human mobility are discussed in the paper.

1. Introduction

Extreme weather event (EWE), such hurricane and flood, by definition is an event that is rare at a particular place and time of year, which would normally be as rare as or rarer than the 10th or 90th percentile of a probability density function estimated from observations (IPCC, 2014). Yet, the world is witnessing a trend of increasing frequency and intensity of EWEs in the past decades (Sobel & Tippett, 2018). For instance, as recent as in 2017, within ten weeks from August to October ten consecutive Atlantic storms reaching hurricane strength hit America, matching a 124-year-old record. Moreover, owing to the impacts of global climate change and sea level rise (Bouwer, 2011; Kelman, Gaillard, & Mercer, 2015 ; Van Aalst, 2006), such trend is projected to continue to escalate (Forzieri et al., 2016; Yin, Yu, Lin, & Wilby, 2017), which highlights the need for knowledge about the growing EWE-induced impacts and enhancement of anticipatory adaptation and resilience.

EWEs, due to their high uncertainty, massive scale, irreversibility and destructiveness, impose significant threats to human wellbeing. Such threats are especially unprecedented in urban regions, which have been the primary bearer of EWE-induced losses due to the high density of population and assets in cities (Hurricane Sandy rebuilding strategy, 2013) and cascading risks associated with complexities of urban systems (Hasan & Foliente, 2015; Mao & Li, 2018; Yang, Ng, Zhou, Xu, & Li, 2019). One remarkable example of such EWE-induced impacts on urban regions, as prior research has revealed, is that during these disasters the mobility patterns of urban population usually exhibit significant variations (Chapman, Nilsson, Larsson, & Rizzo, 2017). These variations involve drastic changes in the intensity and spatiotemporal characteristics of trajectories of urban population. Such variations of urban mobility could be attributed to a variety of factors, such as reduced transportation infrastructure capacities, adverse weather and commuting conditions, interrupted economic activities, and disturbed social dynamics. Hence, they provide a unique angle to examine the overall impact of EWEs that the urban population endures.

Recent research has substantially advanced the knowledge of general human mobility patterns in cities, thanks to the increasing accessibility to various human trajectory data in the form of mobile phones records, GPS traces of vehicles and human beings, and check-ins of online social media. These data have helped researchers to uncover the patterns of human mobility from more perspectives and gain deeper understanding of their underlying mechanisms. Findings of these studies have also been applied to various domains, such as urban planning (Clarry, Imani, & Miller, 2019; Khan, Babar, & Ahmed, 2017; Yuan,

* Corresponding author.
E-mail address: nanli@tsinghua.edu.cn (N. Li).

https://doi.org/10.1016/j.scs.2019.101671
Received 25 March 2019; Received in revised form 7 June 2019; Accepted 18 June 2019
Available online 19 June 2019

Zheng, & Xie, 2012) and transportation management (Gohar, Muzammal, & Rahman, 2018; Pan, Zheng, Wilkie, & Shahabi, 2013). One major gap in the literature, however, is that there is comparatively little understanding of human movements in cities during extreme events such as EWEs (Wang & Taylor, 2014), which has largely prevented the prediction and mitigation of EWE-induced impacts on urban population. To advance this line of research, academics would benefit from having proper metrics that assess (1) how human mobility patterns are perturbed by EWEs and to what extent, and (2) how such perturbation varies over the timespan of EWEs. In practice, cities would be enabled by a perturbation assessment tool (1) to predict human mobility perturbation, and warn the impacted population ahead of the EWEs; (2) to monitor the EWE-induced impacts with real-time trajectory data, and take informed measures to mitigate the impacts; and (3) to conduct quantitative post-event assessment of the EWE-induced impacts on urban population, and learn from the impact assessment to develop adaptive capacities to withstand similar events in the future.

To contribute to the existing knowledge about perturbations that EWEs may cause to urban human mobility, this paper reports findings and lessons learned from a case study in Nanjing, China. A major city in China with a population of 8.3 million, Nanjing recently experienced a rainstorm in June 2017 and a snowstorm in January 2018. Both events broke the city's meteorological record in decades, and caused significant impacts on human mobility in the city. The objective of this case study is to quantitatively assess the human mobility perturbation caused by these two events. To achieve this objective, this case study collected the trajectories of all buses and taxis in Nanjing in periods covering the rainstorm and snowstorm events. Both bus trajectories (Jiang, Guan, Zhang, Chen, & Yang, 2017; Liu et al., 2017) and taxi trajectories (Tang, Liu, Wang, & Wang, 2015; Zheng, Rasouli, & Timmermans, 2016) are widely used for studying urban human mobility in the literature, and are considered indicative of the trends of city-wide human mobility (Wang, Yang, Sun, & Gao, 2017; Wang, Wang, & Taylor, 2017). Based on the collected trajectories, the case study measures both the instantaneous perturbation at any given moment during an EWE, and the accumulated perturbation over the entire timespan of the EWE, using two different metrics. It is anticipated that the findings and lessons learned would help decision makers of cities to better understand the mobility pattern of urban population impacted by EWEs, and develop informed and effective policies and measures to enhance the resilience of cities to EWE-induced impacts.

2. Related work

2.1. Measurement of human mobility

Driven by the rising awareness that understanding of human mobility can bring significant value to various applications such as urban planning (Yuan et al., 2012), traffic management (Pan et al., 2013) and epidemiology (Balcan et al., 2009), there is an increasing volume of literature that examines human mobility in cities. Measuring human mobility, namely quantifying human trajectories recorded in different forms with certain metrics, is the prerequisite of analyzing the statistical characteristics of human mobility and understanding its patterns. For human mobility measurement purpose, a few metrics have been proposed in prior research. These metrics can be broadly divided into two categories, which respectively measure the spatial and temporal characteristics of human mobility.

To measure the spatial characteristics of human mobility, displacement (aka flight length, jump length or trip) is a widely used metric. Displacement is defined as the distance between two consecutive locations which an individual travels (Wang & Taylor, 2016). Measurement of displacement has been widely used in human mobility modeling and analysis research (Barbosa et al., 2018; Brockmann, Hufnagel, & Geisel, 2006; Gonzalez, Hidalgo, & Barabasi, 2008). Studies found that there was power law distribution between displacement and its frequency based on circulation data of bank notes (Brockmann et al., 2006) and call detail record (CDR) data (Gonzalez et al., 2008), and exponential distribution or segmentation combinations of multiple distributions based on GPS data in public transportation (Liang, Zheng, Lv, Zhu, & Xu, 2012; Roth, Kang, Batty, & Barthelemy, 2011; Wang, Huang, & Yan, 2012). A variation of displacement is speed and directions of movements (Kim, Kotz, & Kim, 2006), from which certain characteristics that reflect human mobility patterns could also be obtained. Another common metric for human mobility quantification is Mean Square Displacement (MSD), which can be calculated as the average squared displacements of individuals after a time period. MSD reflects the type of diffusion of individuals relative to their starting points in a trip (Barbosa et al., 2018). Radius of gyration is another metric introduced in prior research (Wang & Taylor, 2018). Defined as the root mean square distance of points from a given axis (Barbosa et al., 2018), radius of gyration characterizes how far an individual is from the center of the mass of his movements. Radius of gyration is also generally believed to follow a power law distribution (Gonzalez et al., 2008). Individuals with comparable radius of gyration usually share certain similarities in their mobility, hence, several studies were able to use this metric to classify mobile individuals into different groups to further study their respective mobility patterns (Oliveira, Viana, Sarraute, Brea, & Alvarez-Hamelin, 2016).

On the other hand, a number of studies have focused on the temporal characteristic of human mobility. Transfer time is a widely used metric for this purpose (Papandrea et al., 2016). It is defined as the time needed to move from one point to another. Other common metrics include pause time (aka interval time) (Rhee et al., 2011), which refers to the interval time between an individual's continuous behaviors such as between mobile phone calls, and waiting time (aka visiting time, contact time or duration) (Oliveira et al., 2016), which refers to the time of an individual staying at a certain place or the completion time of a certain task. Points of interest (PoIs), which refer to places visited by an individual, are important in understanding the human mobility characteristics. A metric of relevance (R), defined as the proportion of time which a given PoI has been visited by an individual, is used to measure the importance of PoIs and classify people that visit them (Papandrea et al., 2016). A small number of important PoIs, such as home, workplace and school, usually take up most of the time. Researchers also ranked PoIs by frequency of visits and found that there was a Zipf law between the rank of the PoIs and the frequency of visits (Gonzalez et al., 2008). Moreover, the understanding of temporal characteristic of human mobility makes the prediction of human movement possible (Oliveira et al., 2016; Papandrea et al., 2016). For prediction purpose, it is important to measure the randomness of human trajectories, for which the concept of entropy is introduced (Lu, Wetter, Bharti, Tatem, & Bengtsson, 2013; Song, Qu, Blumm, & Barabási, 2010). Examples of entropy-related metrics proposed in the literature include random entropy, which captures the degree of predictability of an individual's whereabouts when assuming each location is visited with equal probability, temporal-uncorrelated entropy, which reflects the characteristics of the heterogeneity of visitation patterns, and actual entropy, which captures the full spatiotemporal order of the mobility pattern of an individual (Lu et al., 2013; Song et al., 2010).

2.2. Human mobility perturbation under extreme events

Thus far, only a few studies have explored human mobility during disaster times. Most of these studies found that human mobility would be significantly perturbed by disasters. For instance, Lu, Bengtsson, and Holme (2012) examined the cumulative distributions of displacements and radius of gyration for residents in Port-au-Prince after the 2010 Haiti earthquake, and found that these distributions changed significantly during disaster times. Based on geo-tagged twitter data, Wang and Taylor (2014) also found that the distributions of displacements of residents in New York City significant changed during

Hurricane Sandy. They further explored human mobility patterns under different disaster events and found that the power law distribution dominated human mobility in most cases (Wang & Taylor, 2016). However, most of these studies stopped short of assessing the human mobility perturbation with quantitative metrics.

In addition, several studies noticed the temporal characteristics of human mobility perturbation over the timespan of disaster events. One example is the study conducted by Yabe, Tsubouchi, Sudo, and Sekimoto (2016), in which the researchers calculated the average movement of individuals in regions impacted by Kumamoto Earthquake using smartphone GPS data. They found that the movement increased in the immediate aftermath of the earthquake but then decreased over time. Similarly, and Wang, Wang et al. (2017) studied the impact of a severe winter storm on human mobility in the northeastern United States during thirty-five 24 -h periods, and reported that the percentages of short trips (8–100 meters) and long trips (10 km or more) varied from Monday to Friday differently during the storm than during normal weeks. In another study done by Wang and Taylor (2017), the researchers used Fisher information and network metrics, such as number of edges, number of vertices, and average degree, in human mobility networks to study the perturbation of human mobility during a flood event. The daily variations of these metrics from ten days before the event to ten days after the event were illustrated, which suggested that the human mobility perturbation was highly dynamic, although such dynamics or the accumulated perturbation over time were not quantitatively assessed.

2.3. Gaps in measuring human mobility perturbation

Despite the above studies that have attempted to report and assess the perturbation of urban human mobility, there still lacks proper metrics for quantitatively assessing human mobility perturbation caused by EWEs or other extreme events alike. Several metrics that were introduced in prior research and could be used for this purpose are either indirectly indicative (e.g. displacement and its variations), cannot be interpreted physically (e.g. variables in data driven human mobility models), or are not normalizable and hence cannot be used as benchmark (e.g. complex network metrics). Moreover, the perturbation of human mobility during extreme events is usually dynamic, with changing magnitudes and other complex temporal characteristics. Yet, none of the existing metrics can capture the temporal variation of the perturbation and measure the overall impact of EWEs on human mobility over the entire timespan of the events. The lack of human mobility perturbation metrics has prevented deep understanding of human mobility perturbation during EWEs and the development of proper measures to mitigate such adverse impacts. In addition, although various types of trajectory data have become available for human mobility studies in recent years, prior research on human mobility during extreme events has mostly relied on CDR or social media check-in data, which are relatively sparse in time and space. It may be possible to capture and assess the EWE-induced perturbation of human mobility at a higher granularity when denser trajectory data, such as continuous GPS tracking data, are used.

3. Case study in Nanjing

3.1. Case descriptions

3.1.1. Rainstorm and snowstorm events

Nanjing is the provincial capital of Jiangsu, China, with a total population of over eight million people. On June 10, 2017, the city experienced a major rainstorm. The city issued a red flag warning, which was the highest warning level set by China Meteorological Administration (CMA), meaning the rainstorm is causing or probably going to cause flooding and ground transportation interruptions, and people are advised to stay indoors (China Meteorological Administration, 2018). The rainstorm lasted for around one day with a total precipitation of more than 210 mm, setting a new meteorological record of the city in 66 years (Xinhua, 2017). The peak hourly rainfall far exceeded the threshold of the highest level of intensity of rainfall ("heavy", over 7.6 mm per hour) according to the classification of American Meteorological Society (AMS, 2012).

About seven months later, the city was caught in another EWE. Beginning on January 24, 2018, a snowstorm hit Nanjing and lasted intermittently for almost four days. It was the heaviest snowfall in the city in the past ten years, with around 40 mm of snow water equivalent (SWE). China's National Observatory issued an orange flag snowstorm warning on January 25, 2018 (Xinhua, 2018), which was the second highest warning level of snowstorms set by CMA, meaning the snowstorm is causing or probably going to cause major impacts on transportation and agriculture, and people are advised to stay indoors (China Meteorological Administration, 2015). A large number of buses were forced to stop operation or take detours, and the airport of the city was temporarily shut down (China Central Television, 2018). Based on precipitation records obtained from the provincial meteorological bureau, the hourly rainfall and snowfall (SWE) in the city during the above two EWEs are depicted in Figs. 1 and 2, respectively.

3.1.2. Trajectory data

As regulated, every bus and every taxi in Nanjing is equipped with a

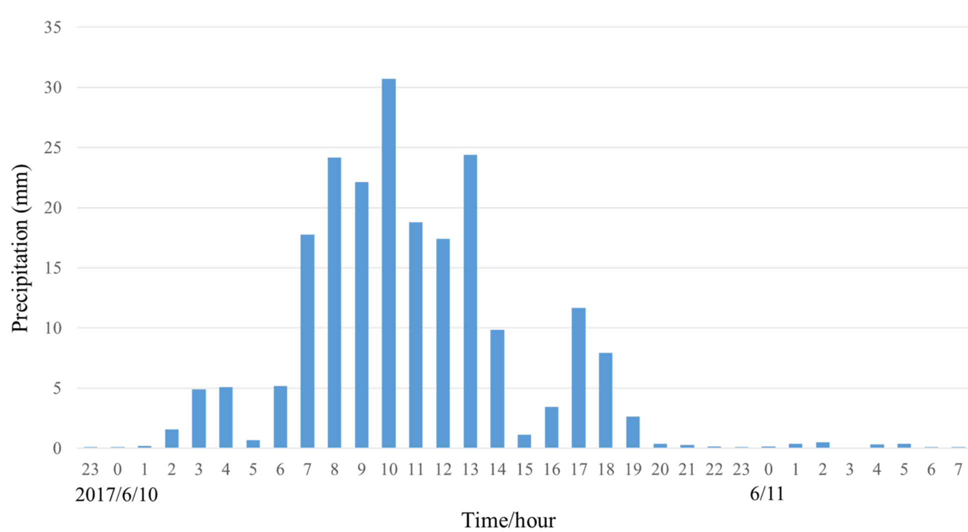

Fig. 1. Hourly precipitation during the rainstorm.

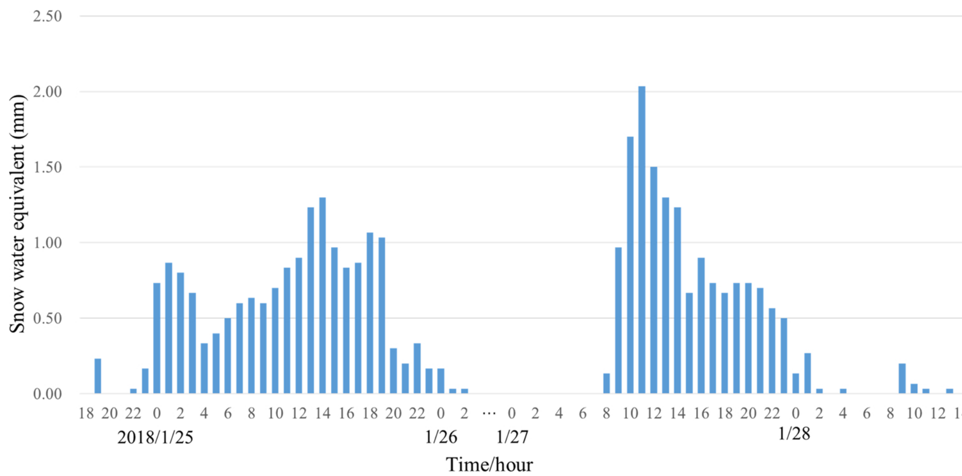

Fig. 2. Hourly snow water equivalent during the snowstorm.

Table 1
Examples of bus trajectory data entries.

Bus ID	Timestamp	Longitude	Latitude
112*	2017/12/5 10:00:08	118.798000	32.087540
112*	2017/12/5 10:00:18	118.798900	32.086930
112*	2017/12/5 10:00:28	118.799500	32.086680
237*	2018/1/13 3:27:06	118.817183	32.101106
237*	2018/1/13 3:27:16	118.816605	32.101149
237*	2018/1/13 3:27:26	118.816296	32.101144

Table 2
Examples of taxi trajectory data entries.

Taxi license plate number	Timestamp	Longitude	Latitude
A7535*	170610080206	118.788020	31.995780
A7535*	170610080213	118.788940	31.995180
A7535*	170610080222	118.789930	31.994480
AB385*	170606001202	118.807760	32.037212
AB385*	170606001214	118.807610	32.037804
AB385*	170606001226	118.806790	32.037770

sensor, which is configured to report to a central server approximately every ten seconds during operation. The reporting contains a number of data fields, the ones relevant to trajectories being vehicle ID, timestamp, longitude and latitude. Tables 1 and 2 show a few examples of raw data entries of the buses and taxis trajectories, respectively. The bus trajectory data were collected from May 1, 2017 to June 30, 2017 and from December 1, 2017 to February 4, 2018, which covered 6848 buses and included more than three billion data entries. The taxi trajectory data were collected from May 1, 2017 to June 30, 2017, which covered 12,432 taxis and included more than one and a half billion data entries. These data were cleaned, by filtering corrupted entries caused by sensor malfunctions and merging duplicate entries, and prepared for analysis of human mobility perturbation in the city.

National and local media outlets reported that these two EWEs and the associated inundation and low visibility resulted in serious capacity reductions of numerous segments in the road network, caused significant city-wide traffic congestions, and severely impacted the overall commuting conditions in the city. Many residents were forced to stay indoors, and various municipal services including public transportation were interrupted (Lu, 2018; Wang, 2017).

This case study aims to assess the impacts of these two EWEs on the human mobility in Nanjing. Specifically, this case study aims to measure both the instantaneous perturbation at any given moment during an EWE, and the accumulated perturbation over the entire timespan of the EWE, so as to provide a comprehensive account of the deviation between human mobility during EWE and its normal state in the case city.

3.2. Methods

3.2.1. Assessment of human mobility perturbation

In order to measure the instantaneous perturbation at any given moment during an EWE, a proper metric is needed. This metric should be physically meaningful, computable, and comparable. Physically meaningful means the metric should be derived from or interpretable into variables in physics based models, rather than data driven models, therefore it can be theoretically explained and acted upon in reality; Computable means the computation of the metric should be feasible based on available form of human trajectory data; Comparable means the value of the metric should have clear boundaries, and it can be normalized so as to allow for benchmarking between different scenarios. Based on the above criteria, a metric termed relative total displacement (*RTD*) is introduced as follows:

First of all, as aforementioned, displacement (d) is one of the most widely used metrics for measuring human mobility based on human trajectories. By accumulating a series of consecutive displacements traveled by all individuals in question (in this case study, an individual refers to either a bus or a taxi), total displacement (*TD*) can be calculated. Adapted from vehicle miles traveled (VMT), a metric widely used in the transportation domain (Ewing & Cervero, 2010), *TD* can be calculated based on Eq. (1):

$$TD = \sum_{j=1}^{m} \sum_{i=1}^{n-1} d_{ij} \tag{1}$$

where m is the number of individuals, n is the number of locations the j-th individual visits during a timespan (e.g. an hour), and d_{ij} is the i-th displacement in the trajectory of the j-th individual, which can be computed based on Eq. (2) (Wang & Taylor, 2016):

$$d_{ij} = 2r \times \sin^{-1}\left(\sqrt{\sin^2(\frac{\theta_{i+1,j} - \theta_{i,j}}{2}) + \cos\theta_{i+1,j}\cos\theta_{i,j}\sin^2(\frac{\varphi_{i+1,j} - \varphi_{i,j}}{2})}\right) \tag{2}$$

where r denotes the radius of the earth, $\theta_{i,j}$ and $\varphi_{i,j}$ denote the latitude and longitude of the first point of the i-th displacement in the trajectory of the j-th individual in radians, and $\theta_{i+1,j}$ and $\varphi_{i+1,j}$ denotes the latitude and longitude of the second point of the i-th displacement in the trajectory of the j-th individual in radians.

TD accounts for two parts of influence that EWEs may have on human trajectories, including reduced travel speed and hence smaller displacement of operating buses and taxis due to poor road conditions and abnormal traffic congestion, and non-operation of buses and taxis due to inaccessibility to service in certain areas or change of work schedules during EWEs. After *TD* is calculated, a baseline is needed in order to assess the deviation of *TD* from its normal state, namely the level of perturbation of human mobility. The baseline, denoted as $\overline{TD}$, measures the total displacement of all individuals during a timespan should the EWE not happen. $\overline{TD}$ can be calculated based on *TD* values under normal conditions. For a given timespan (e.g. an hour) during an EWE, assuming it shares with *n* timespans that are under normal conditions the same circumstances that could possibly impact human mobility, except the weather condition, then its $\overline{TD}$ value can be calculated as:

$$\overline{TD} = \sum_{i=1}^{n} TD_i \tag{3}$$

where TD_i is *TD* value of the *i*-th timespan under normal conditions. Based on the TD_i value, *RTD* can be calculated by normalizing *TD* with $\overline{TD}$, as shown in Eq. (4):

$$RTD = \frac{TD}{\overline{TD}} \times 100\% \tag{4}$$

RTD is a normalized metric that measures the deviation of actual human mobility during an EWE from its normal state, and is therefore a reasonable metric for assessing the magnitude of instantaneous EWE-induced human mobility perturbation.

3.2.2. Assessment of accumulated perturbation impacts on human mobility

As an EWE develops throughout its entire timespan, its characteristics change, leading to variations in its impacts. These variations, coupled with the fact that urban population tend to adapt to EWE-induced impacts by dynamically adjusting their travel preferences and behaviors (Zanni & Ryley, 2015), may cause human mobility perturbation to be highly fluctuant. It is therefore important to track the fluctuations and evolution of human mobility, and assess the accumulated perturbation impacts throughout the entire timespan of the EWE.

During the timespan of an EWE, human mobility begins to be perturbed when it is impacted by the EWEs, and this perturbation lasts for a certain period of time until the impact of EWE fades away. Motivated by the resilience concept and resilience quantification framework (Cimellaro, Reinhorn, & Bruneau, 2010), the evolution of human mobility perturbation can be depicted in a curve (e.g. Fig. 3) to visually illustrate the impacts of EWEs on the mobility of urban population.

Moreover, since human mobility perturbation can be measured by a normalized variable *RTD*, whose value varies between [0,1], integrating *RTD* over the timespan of an EWE will yield a normalized metric for assessing the accumulated perturbation (*AP*) of human mobility:

$$AP = \int_{t_0}^{t_1} \frac{1 - RTD}{t_1 - t_0} dt = 1\text{-} \int_{t_0}^{t_1} \frac{RTD}{t_1 - t_0} dt \tag{5}$$

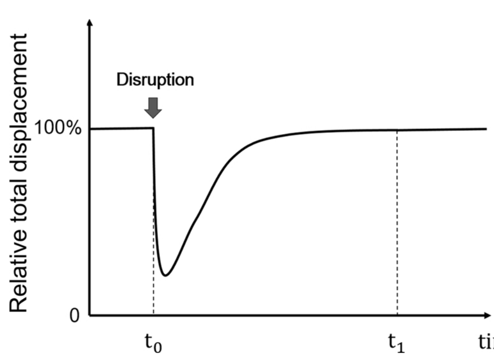

Fig. 3. Curve of human mobility perturbation.

where t_0 denotes the moment of occurrence of perturbation, and t_1 denotes the moment of full restoration of human mobility.

The value of *AP* is determined not only by the magnitude of human mobility perturbation, but also by the duration of EWE impacts. This duration may exceed the timespan of the EWE and last for considerably longer time, and is therefore particularly important in the assessment of overall EWE-induced human mobility perturbation. It needs to be pointed out that t_0 and t_1 are not necessarily equal to the beginning ($t_0^{'}$) and end ($t_1^{'}$) of an EWE. Based on Eq. (2), to calculate *AP* it is important to determine the value of t_0 and t_1. It is proposed in this study that t_0 should be the moment when the *RTD* value first drops below 95% of the baseline; t_1 should be the first point of time after which the hourly *RTD* value remains above 95% for at least the following 24 h, so as to ensure that by time t_1 the impacts of EWE have completed faded away and the human mobility has fully and stably bounced back to its normal pattern.

3.2.3. Metrics computation in the case study

Using bus trajectories and one-hour timespan as an example, *TD* was calculated in the case study in the following steps. First, the trajectory of each bus within a given hour was obtained from the trajectory dataset and organized in chronological trajectory sequence as follows: *[[Bus ID, [longitude1, latitude1], [longitude 2, latitude 2], …, [longitude n, latitude n]]*. Next, the displacement between every two adjacent coordinates in the trajectory sequence was calculated. Then, the hourly displacement of each bus was computed by accumulating all displacements obtained from the trajectory sequence, and *TD* was computed by accumulating the hourly displacement of all buses in the city. The *TD* for taxis was calculated similarly. Due to possible sensor errors, there could be erroneous data and outliers in the *TD* values. A screening rule was applied to eliminate outliers, where the hourly *TD* of a bus or a taxi exceeded 80 km or 120 km, since values above these thresholds were highly unlikely given the normal traffic conditions in the city.

$\overline{TD}$ was calculated on an hourly basis. Considering the obvious daily periodicity (e.g. peak hours of a day) and weekly periodicity (e.g. differences between working days and weekends), the hourly $\overline{TD}$ value was determined based on the mean value of *TD* of the same hour of the same day over five weeks preceding or succeeding the week of the EWEs.

The reliability of this baseline depends on the assumption that under normal weather condition, given the time of the day and the day of the week, the *TD* value is invariant between different weeks. To assess the reliability of $\overline{TD}$, the above assumption was tested by assessing the level of similarity between *TD* of different weeks. Specifically, the difference of *TD* values between weeks *i* and *j* was calculated based on Eq. (6):

$$\Delta d_{ij} = \frac{\sqrt{\sum_{k=1}^{n} (TD_k^i - TD_k^j)^2}}{n} \Bigg/ \frac{\sum_{k=1}^{n} TD_k^i + \sum_{k=1}^{n} TD_k^j}{2n} \tag{6}$$

where TD_k^i and TD_k^j denote *k*-th hourly *TD* value of week *i* and week *j*, respectively, and *n* denotes the number of hours in a week. The *TD* values of all five baseline weeks are plotted in Figs. 4–6, and the differences between these weeks calculated based on Eq. (6) are summarized in Tables 3–5.

As can be seen in Figs. 4–6 and Tables 3–5, the hourly *TD* values were highly consistent across the five weeks. Moreover, the differences of *TD* between any two weeks were all below 0.5%. These results showed that the hourly *TD* values were highly stable under normal conditions, and $\overline{TD}$ calculated in this case study could provide a reliable baseline for following assessment and analysis of urban human mobility perturbation.

In addition, based on the aforementioned criterion, t_1 was calculated to be 23:00, June 10, 2017 for bus trajectories and 3:00, June 11, 2017 for taxi trajectories during the rainstorm event, and 20:00, January 31, 2018 for bus trajectories during the snowstorm event. After these times,

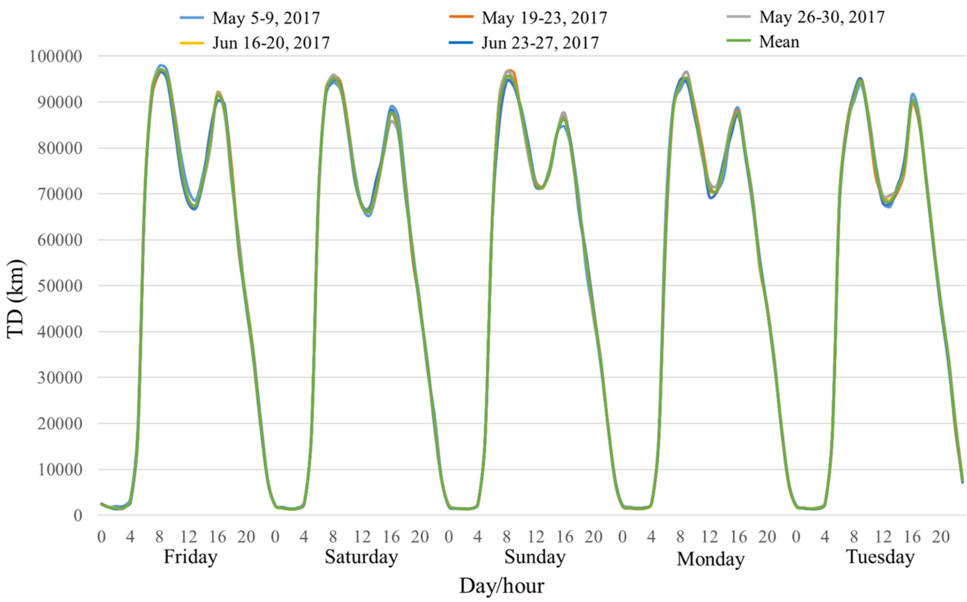

Fig. 4. TD values of bus trajectories for five weeks near rainstorm.

the urban human mobility in Nanjing, assessed based on respective trajectory data, had fully returned to its normal state and remained stable afterwards.

4. Results

The human mobility perturbation in Nanjing during the rainstorm and snowstorm events was assessed using the aforementioned metrics in this case study. The results are summarized in Table 6. It needs to be noted that all calculation and analysis were repeated twice in this study, in which the *TD* values were computed on an hourly basis and a 15-minutely basis, respectively. The results were fairly consistent, indicating that the time granularity of the *TD* values would not impact any results and conclusions. The results reported below are based on hourly *TD* values. In the remainder of this section, these results are analyzed and interpreted from three angles, including comparison between two EWEs, comparison between two transport modes, and geographical distribution of the perturbation.

4.1. Comparison between different EWEs

The *RTD* curve based on bus trajectories for the rainstorm event is shown in Fig. 7. The rainstorm began at 23:00, June 9, and the perturbation of *RTD* began eight hours later at 7:00, June 10, when the EWE started to show significant impact of on human mobility in the city. The rainstorm lasted for 33 h and had a total precipitation of over 210 mm. During this period, the *RTD* curve reached its lowest point (83.59%) around 13:00, June 10. The rainstorm ended around 7:00, June 11, whereas *RTD* fully and stably recovered at 23:00, June 10. This suggested that the human mobility in Nanjing had already started to restore in the course of the event, when the rainfall began to abate, and since the rainfall was rather small in the last few hours of the event, the human mobility had fully restored to its normal state before the rain completely stopped, showing significant resilience to this EWE. Based on the *RTD* curve and Eq. (5), the *AP* value was calculated to be 0.111, which also indicated that, despite the record-breaking amount of rainfall, the human mobility in Nanjing was not severely impacted.

The *RTD* curve based on bus trajectories for the snowstorm event is

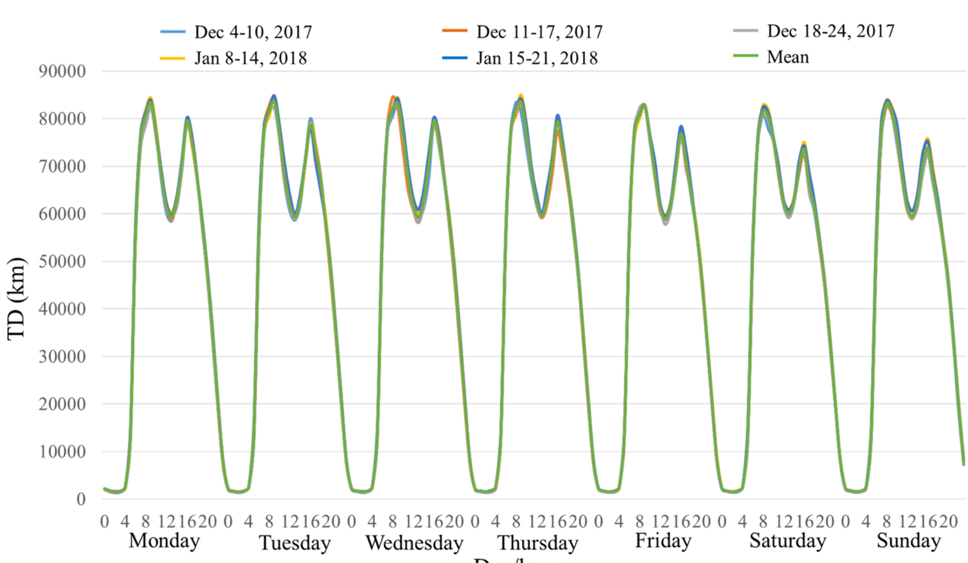

Fig. 5. TD values of bus trajectories for five weeks near snowstorm.

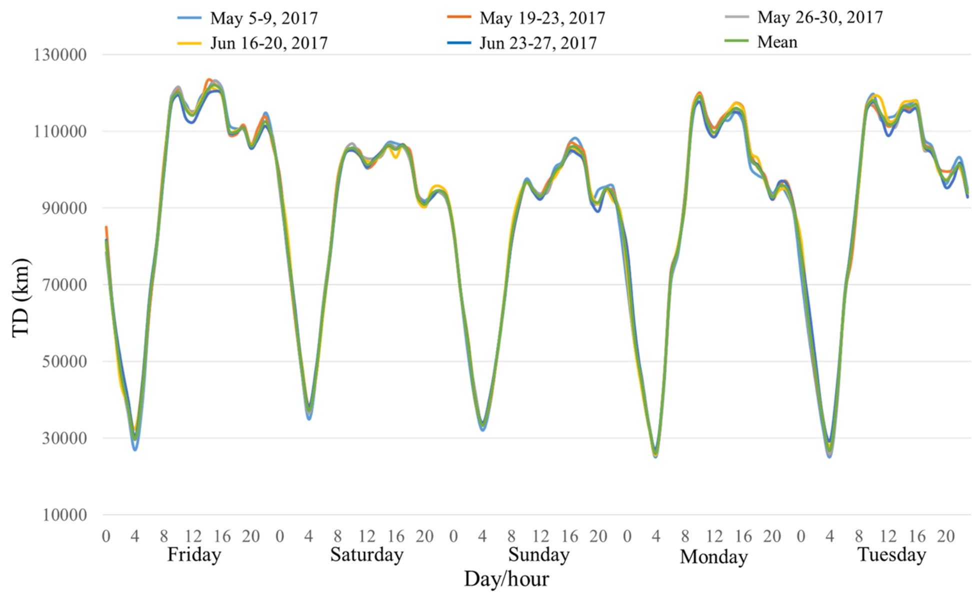

Fig. 6. TD values of taxi trajectories for five weeks near rainstorm.

shown in Fig. 8. As can be seen in the figure, the snowstorm began at 19:00, January 24, and the perturbation of *RTD* began nine hours later at 5:00, January 25. The snow temporarily stopped between 3:00, January 26 and 7:00, January 27, after which the city was met with another wave of snow until 13:00, January 28. During this period, the *RTD* value oscillated significantly exhibiting a W-shape, reaching its low values during the daytime and partially bouncing back at nighttime. The lowest *RTD* value (27.65%), in other words the largest human mobility perturbation, was observed at 7:00, January 26. The relatively higher *RTD* values at nighttime showed that the human mobility was barely perturbed at night, suggesting that the magnitude of instantaneous perturbation may be escalated by increases in the intensity of human mobility. The snowstorm ended at 13:00, January 28, whereas *RTD* fully and stably recovered at 20:00, January 31, indicating that the perturbation of human mobility lasted for an extra 78 h beyond the end of the snowstorm event. The duration of the human mobility perturbation almost doubled the duration of the snowstorm event. Based on the *RTD* curve and Eq. (5), the *AP* value was calculated to be 0.210.

The above results from both EWEs showed that there were significant delays between the occurrence of EWEs (t_0') and appearance of observable perturbation of human mobility (t_0), indicating that the urban population exhibited certain level of resistance to EWEs and was able to absorb their initial impacts in the first few hours. There was significant deviation between the end of EWEs (t_1') and disappearance of human mobility perturbation (t_1) as well, indicating that human mobility may fully recover before or after the end of EWEs, depending on the type and intensity of the events. In addition, the instantaneous human mobility perturbation had larger magnitude and significant oscillation during the snowstorm, compared to during the rainstorm. This suggested that Nanjing, located in the southern and warm region of China, was not well prepared for snowstorms, had relatively high vulnerability to such EWEs, and experienced remarkable impacts in this particular event.

4.2. Comparison between different modes of transport

Other than buses, taxis provide another important mode of transport in the city. Prior studies have found that human mobility based on these two modes of transport had different patterns under normal condition (Jiang et al., 2017). However, when impacted by EWEs, whether and how bus-based and taxi-based human mobility would be perturbed differently remains unknown. To investigate this issue, the *RTD* curve based on taxi trajectories during the rainstorm is illustrated in Fig. 9. While this curve had a similar shape to the *RTD* curve based on bus trajectories, these two curves had several major differences. Firstly, for taxi-based human mobility, the *RTD* value started to decrease almost immediately after the rainstorm started, suggesting that taxi-based human mobility was much more sensitive to EWE impacts. Such sensitivity was also reflected by the fact that *RTD* curve based on taxi trajectories had a lower bottom value of 79.21% and lower *AP* value of 0.145, showing that the rainstorm caused larger perturbation to taxi-based human mobility. This difference was probably because taxis were relatively less regulated than buses, and had more flexibility to choose not to work when weather conditions and road conditions were poor. Bus services, on the other hand, were more regulated by bus companies and local transportation authority, which were motivated to maintain public transportation services during EWEs. Hence, bus services showed higher resilience to EWE impacts, and bus trajectories and bus-based mobility were relatively less perturbed.

4.3. Human mobility perturbation in different subareas

To further analyze the impact of the two EWEs on human mobility

Table 3
Difference of TD values of bus trajectories among five weeks near rainstorm.

	May 5-9, 2017	May 19-23, 2017	May 26-30, 2017	Jun 16-20, 2017	Jun 23-27, 2017
May 5-9, 2017	—				
May 19-23, 2017	0.230%	—			
May 26-30, 2017	0.254%	0.182%	—		
Jun 16-20, 2017	0.155%	0.129%	0.137%	—	
Jun 23-27, 2017	0.241%	0.204%	0.207%	0.139%	—

Table 4
Difference of TD values of bus trajectories among five weeks near snowstorm.

	Dec 4-10, 2017	Dec 11-17, 2017	Dec 18-24, 2017	Jan 8-14, 2018	Jan 15-21, 2018
Dec 4-10, 2017	—				
Dec 11-17, 2017	0.173%	—			
Dec 18-24, 2017	0.149%	0.151%	—		
Jan 8-14, 2018	0.262%	0.255%	0.228%	—	
Jan 15-21, 2018	0.305%	0.289%	0.272%	0.124%	—

in Nanjing, the geographical distribution of the human mobility perturbation was assessed. The city was divided by grids into 144 subareas, each with an area of $5 \times 5\ km^2$. The trajectories that fell into each grid were analyzed to assess the human mobility perturbation within that subarea. Due to less density of trajectories in some subareas, the criterion of determining t_1 was slightly loosened and adjusted as the first point of time after which the hourly *RTD* value of the following 12 h remained to be above 95%.

The results are illustrated in Figs. 10–12. The color in these figures represents the level of human mobility perturbation. Greenish color indicates less perturbation, and reddish color indicates more perturbation. The grey color indicates that there were no or too few trajectories in those subareas to calculate valid *AP* values, and hence the perturbation in those subareas was not assessed. In Fig. 10, the color distribution is relatively uniform and greenish, with little geographical variation, suggesting that the bus services were maintained generally well across the entire city during the rainstorm. In Figs. 11 and 12, there was noticeable difference in color between the southern and northern parts of the city. Most subareas in the south were green while most subareas in the north were yellow and red, which indicated that the southern part of the city was more resilient to the EWEs. Further investigation revealed that the southern part had relatively better economic conditions and it was where many provincial and municipal government agencies were located. Hence, when the snowstorm happened, measures of mitigation and recovery were likely to kick in first in the south. Yet, it should be noted that this may not be the only reason for the above difference. Infrastructure condition, geographical characteristics and distribution of snowfalls and rainfalls might also affect the AP values of the subareas. The above geographical difference would be better interpreted if more contextual data about the urban environments were available.

5. Discussions

The case study demonstrated the efficacy of the proposed metrics. The metrics *RTD* and *AP* were successfully applied to the quantitative assessment of human mobility perturbation during two EWEs in Nanjing, and yielded reasonable assessment results. More importantly, these metrics, which are calculated based on displacements traveled by all individuals in questions, are physically meaningful and can be acted upon in reality. Their application in the case study also proved that the metrics are easily computable based on human trajectories, and that the normalized assessment results can be used for benchmarking between different scenarios. This suggests that the metrics can fulfill the aforementioned objectives of this study, which is to measure both the instantaneous perturbation at any given moment during an EWE, and the accumulated perturbation over the entire timespan of the EWE, with physically meaningful, computable and comparable metrics. By achieving these objectives, this study advances the existing knowledge about human mobility during EWE in several ways. First, while existing literature thus far has mostly focused on descriptive observations of the mobility perturbation, this study develops effective metrics for quantifying the impact of EWEs, which notably enables future exploratory research into this problem, and supports the development of measures, such as improving emergency service accessibility (Yin et al., 2017), to mitigate the adverse impact. Second, this study considers both instantaneous and accumulated impacts of the EWEs. By doing so, it views the perturbation as a dynamic process whose patterns and overall impact can be measured. This highlights a comprehensive angle to explore the characteristics of human mobility perturbation, which can provide a full account of the deviation between human mobility during EWE and its normal state in a city.

Taxi and bus trajectories were used to assess the perturbation in the case study. Admittedly, these trajectories were not perfect representation of the mobility of the entire population in Nanjing. However, they were reasonably representative for several reasons. First, public transport trajectories, especially taxi trajectories, have been widely used to study urban human mobility in prior research (Peng, Jin, Wong, Shi, & Lio, 2012; Tang et al., 2015; Wang, Yang et al., 2017; Yao & Lin, 2016;). The human mobility patterns extracted from taxi trajectories were also found to be similar to those extracted from other types of data, such as private vehicles and mobile phones (Wang, Pan, Yuan, Zhang, & Liu, 2015). Second, people in Nanjing rely heavily on public transport for their mobility. They completed over two billion trips using public transport in 2017, among which bus- and taxi-based trips accounted for 43.16% and 9.49%, respectively (Nanjing Municipal Bureau of Statistics, 2018). Metro, which accounted for another 47.05% of the trips, was much less sensitive than buses or taxies to the impact of EWEs. Therefore, most of the perturbation was observed in bus and taxi trajectories. Lastly, it is noteworthy that, although several transport modes, such as metro, private cars and walking, were not included in the case study, trajectories associated with these transport modes could also be analyzed with the metrics used in this study, should the trajectory data be made available.

There are several limitations in this case study that need to be noted, including that the trajectories were analyzed at the vehicle level rather than the passenger level, due to challenges in obtaining the trajectory data of individual passengers, and that the results were only inclusive of

Table 5
Difference of TD values of taxi trajectories among five weeks near rainstorm.

	May 5-9, 2017	May 19-23, 2017	May 26-30, 2017	Jun 16-20, 2017	Jun 23-27, 2017
May 5-9, 2017	—				
May 19-23, 2017	0.208%	—			
May 26-30, 2017	0.182%	0.150%	—		
Jun 16-20, 2017	0.231%	0.177%	0.158%	—	
Jun 23-27, 2017	0.247%	0.171%	0.153%	0.171%	—

Table 6
Summary of case study results.

	Rainstorm		Snowstorm
	Bus trajectories	Taxi trajectories	Bus trajectories
Beginning of EWE (t_0‘)	23:00, Jun 09, 2017	23:00, Jun 09, 2017	19:00, Jan 24, 2018
Beginning of mobility perturbation (t_0)	7:00, Jun 10, 2017	00:00, Jun 10, 2017	5:00, Jan 25, 2018
End of EWE (t_1’)	7:00, Jun 11, 2017	7:00, Jun 11, 2017	13:00, Jan 28, 2018
End of mobility perturbation (t_1)	23:00, Jun 10, 2017	3:00, Jun 11, 2017	20:00, Jan 31, 2018
The lowest *RTD* value	83.59%	79.21%	27.65%
AP value	0.111	0.145	0.210

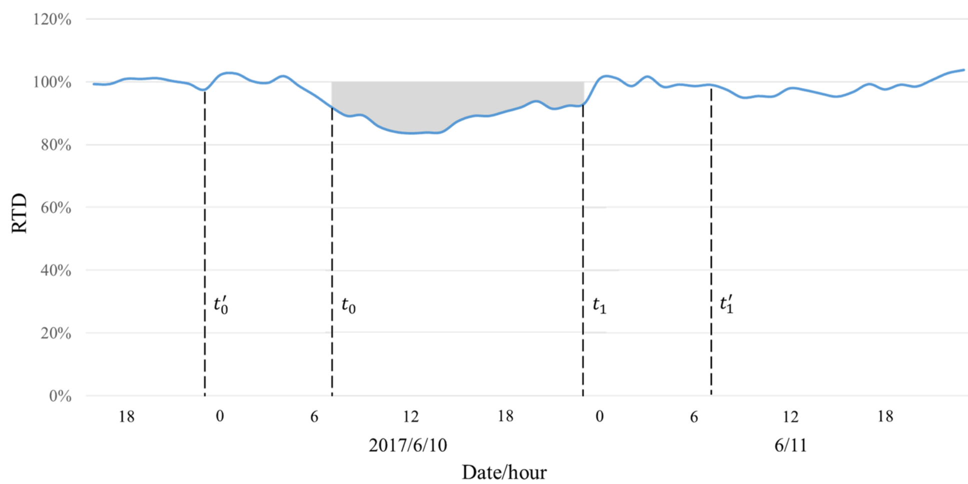

Fig. 7. RTD curve based on bus trajectories during the rainstorm event.

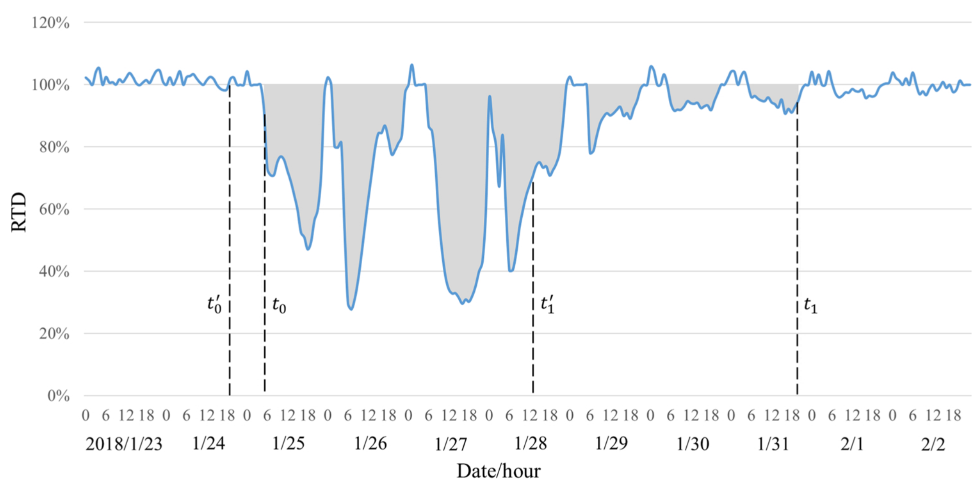

Fig. 8. RTD curve based on buses trajectories during the snowstorm event.

transport modes of buses and taxis. Future research could further look into mobility perturbation at higher granularity and from more diverse transport modes, examine underlying impact factors of the perturbation, and develop approaches for predicting and intervening the perturbations during EWEs. In addition, future research should also look into certain types of non-extreme events, such as nuisance flooding (Moftakhari, Aghakouchak, Sanders, Allaire, & Matthew, 2018), that can cause minor but frequent and widespread perturbation to urban human mobility.

6. Conclusions

This paper reports a case study that aimed to investigate the human mobility perturbation in urban regions during EWEs. The findings indicated that urban population had certain level of resistance to EWEs and was able to absorb their initial impacts. The human mobility pattern would begin to restore in the course of the event, and may fully restore to its normal state before the event completely ends. The findings also indicated that the snowstorm caused more significant, oscillating and lasting perturbation to human mobility in Nanjing than the rainstorm. The perturbation was more significant in subareas of the city that were relatively less developed and likely less swift in mobilizing resources for disaster impact mitigation.

The findings from the case study have important practical implications for cities. By understanding the magnitude of EWE-induced perturbation to urban human mobility, and the temporal and geographical distribution patterns of the perturbation, decision makers in cities can take proper measures to mitigate these impacts. Examples of

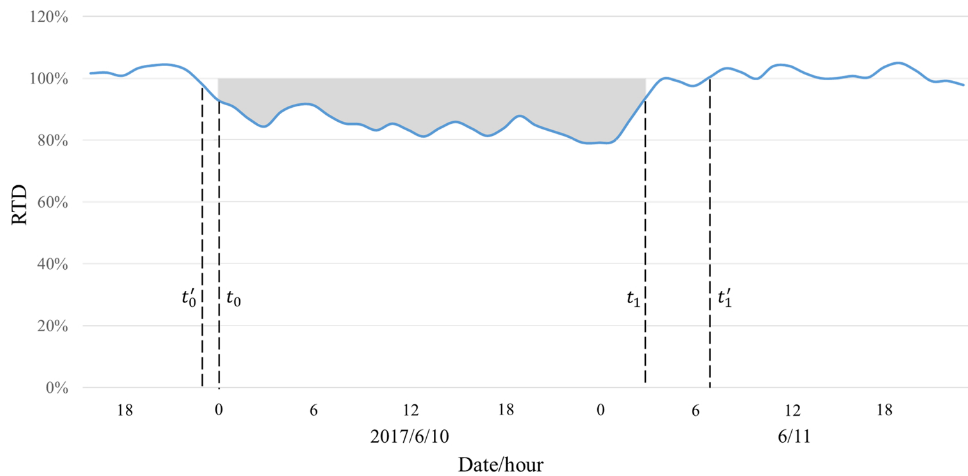

Fig. 9. RTD curve based on taxi trajectories during the rainstorm event.

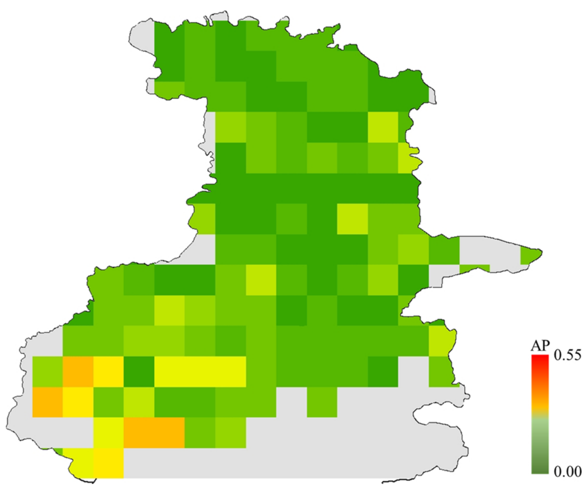

Fig. 10. AP values of subareas based on bus trajectories during the rainstorm.

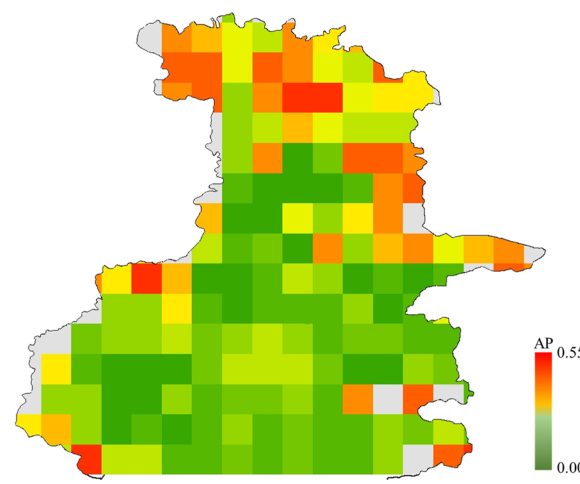

Fig. 12. AP values of subareas based on taxi trajectories during the rainstorm.

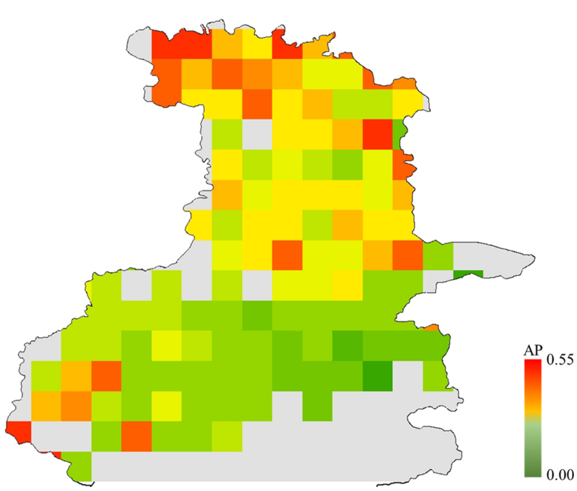

Fig. 11. AP values of subareas based on bus trajectories during the snowstorm.

such measures include pre-event evacuation of the most vulnerable population, and resource mobilization to support the recovery of the most impacted regions. Moreover, cities that have different situations or are faced with distinct threats of EWEs can utilize the metrics introduced in this study to conduct their own assessment, which would lay the basis for more informed and effective policies and measures to improve the adaptive capacities of cities to withstand EWE-induced impacts in the future.

Declaration of Competing Interest

None.

Acknowledgments

This material is based on work supported by the National Key R&D Program of China under Grant No. 2017YFC0803300, and National Natural Science Foundation of China (NSFC) under Grant No. U1709212. The authors are grateful for the support of the Ministry of Science and Technology (MOST) of China and NSFC. Any opinions, findings, and conclusions or recommendations expressed in this paper are those of the authors and do not necessarily reflect the views of the funding agencies.

References

AMS (2012). *Glossary of meteorology. American meteorological society*. Accessed 10 November 2018: http://glossary.ametsoc.org/wiki/Rain.

Balcan, D., Colizza, V., Gonçalves, B., Hu, H., Ramasco, J. J., & Vespignani, A. (2009). Multiscale mobility networks and the spatial spreading of infectious diseases. *Proceedings of the National Academy of Sciences, 106*, 21484–21489.

Barbosa, H., Barthelemy, M., Ghoshal, G., James, C. R., Lenormand, M., Louail, T., et al. (2018). Human mobility: Models and applications. *Physics Reports, 734*, 1–74.

Bouwer, L. M. (2011). Have disaster losses increased due to anthropogenic climate change? *Bulletin of the American Meteorological Society, 92*, 39–46.

Brockmann, D., Hufnagel, L., & Geisel, T. (2006). The scaling laws of human travel.

Nature, 439, 462–465.
Chapman, D., Nilsson, K., Larsson, A., & Rizzo, A. (2017). Climatic barriers to soft-mobility in winter: Luleå, Sweden as case study. *Sustainable Cities and Society, 35C*, 574–580.
China Central Television (2018). *Impacted by Severe Snowstorm, Nanjing Lukou International Airport was Shut Down, With Cancellation of Over 300 Flights.* Accessed 23 May 2019: http://news.cctv.com/2018/01/27/ARTIrOiAfVRjorcm26KQrg58180127.shtml.
China Meteorological Administration (2015). *Snowstorm warning science.* Accessed 23 May 2019:http://www.cma.gov.cn/yjkp/201506/t20150609_284829.html.
China Meteorological Administration (2018). *How to read the rainstorm warning.* Accessed 23 May 2019:http://www.cma.gov.cn/kppd/kppdrt/201606/t20160612_313796.html.
Clarry, A., Imani, A. F., & Miller, E. J. (2019). Where we ride faster? Examining cycling speed using smartphone GPS data. *Sustainable Cities and Society, 49*, 101594.
Cimellaro, G. P., Reinhorn, A. M., & Bruneau, M. (2010). Framework for analytical quantification of disaster resilience. *Engineering Structures, 32*, 3639–3649.
Ewing, R., & Cervero, R. (2010). Travel and the built environment. *Journal of the American Planning Association, 76*(3), 265–294.
Forzieri, G., Feyen, L., Russo, S., Vousdoukas, M., Alfieri, L., Outten, S., et al. (2016). Multi-hazard assessment in Europe under climate change. *Climatic Change, 137*, 105–119.
Gohar, M., Muzammal, M., & Rahman, A. U. (2018). SMART TSS: Defining transportation system behavior using big data analytics in smart cities. *Sustainable Cities and Society, 41*, 114–119.
Gonzalez, M. C., Hidalgo, C. A., & Barabasi, A. L. (2008). Understanding individual human mobility patterns. *Nature, 453*, 779–782.
Hasan, S., & Foliente, G. (2015). Modeling infrastructure system interdependencies and socioeconomic impacts of failure in extreme events: Emerging R&D challenges. *Natural Hazards, 78*, 2143–2168.
Hurricane Sandy rebuilding strategy (2013). *Hurricane sandy rebuilding task force.* Washington DC. Accessed August 2013:https://www.wnyc.org/static/resources/2013/Aug/19/Hurricane_Sandy_Rebuilding_Strategy.pdf.
IPCC (2014). Annex II: Glossary. In K. J. Mach, S. Planton, & C. von Stechow (Eds.). *Climate change 2014: Synthesis report. Contribution of working groups I, II and III to the Fifth assessment report of the intergovernmental panel on climate change* (pp. 117–130). Geneva, Switzerland: IPCC.
Jiang, S., Guan, W., Zhang, W., Chen, X., & Yang, L. (2017). Human mobility in space from three modes of public transportation. *Physica A, 483*, 227–238.
Xinhua (2018). *Torrential rain leaves six dead, three missing in China.* Accessed 5 November 2018: http://www.chinadaily.com.cn/china/2017-06/11/content_29700732.htm.
Kelman, I., Gaillard, J. C., & Mercer, J. (2015). Climate change's role in disaster risk reduction's future: Beyond vulnerability and resilience. *International Journal of Disaster Risk Science, 6*, 21–27.
Khan, M., Babar, M., & Ahmed, S. H. (2017). Smart city designing and planning based on big data analytics. *Sustainable Cities and Society, 35*, 271–279.
Kim, M., Kotz, D., & Kim, S. (2006). Extracting a mobility model from real user traces. *Proceedings of the 25th IEEE International Conference on Computer Communications,* 1–13.
Liang, X., Zheng, X., Lv, W., Zhu, T., & Xu, K. (2012). The scaling of human mobility by taxis is exponential. *Physica a-Statistical Mechanics and Its Applications, 391*(5), 2135–2144.
Liu, Y., Liu, C., Yuan, N., Duan, L., Fu, Y., Xiong, H., et al. (2017). Intelligent bus routing with heterogeneous human mobility patterns. *Knowledge and Information Systems, 50*, 383–415.
Lu, H. (2018). *Heavy snow disrupts traffic in parts of China.* Accessed 12 November 2018:http://www.xinhuanet.com/english/2018-01/25/c_136924984.htm.
Lu, X., Bengtsson, L., & Holme, P. (2012). Predictability of population displacement after the 2010 Haiti earthquake. *Proceedings of the National Academy of Sciences of the United States of America, 109*, 11576–11581.
Lu, X., Wetter, E., Bharti, N., Tatem, A. J., & Bengtsson, L. (2013). Approaching the limit of predictability in human mobility. *Scientific Reports, 3*, 2923.
Mao, Q., & Li, N. (2018). Assessment of the impact of interdependencies on the resilience of networked critical infrastructure systems. *Natural Hazards* ***93***, 315–337.
Moftakhari, H. R., Aghakouchak, A., Sanders, B. F., Allaire, M., & Matthew, R. A. (2018). What is nuisance flooding? Defining and monitoring an emerging challenge. *Water Resources Research, 54*, 4218–4227.
Nanjing Municipal Bureau of Statistics (2018). *The way people travel in Nanjing is quietly adjusting and changing.* Accessed 23 May 2019:http://221.226.86.104/file/2018/jiaotongyunshu/8-9.htm.
Oliveira, E. M. R., Viana, A. C., Sarraute, C., Brea, J., & Alvarez-Hamelin, I. (2016). On the regularity of human mobility. *Pervasive and Mobile Computing, 33*, 73–90.
Pan, B., Zheng, Y., Wilkie, D., & Shahabi, C. (2013). Crowd sensing of traffic anomalies based on human mobility and social media. *Proceedings of the 21st ACM SIGSPATIAL International Conference on Advances in Geographic Information Systems,* 344–353.
Papandrea, M., Jahromi, K. K., Zignani, M., Gaito, S., Giordano, S., & Rossi, G. P. (2016). On the properties of human mobility. *Computer Communications, 87*, 19–36.
Peng, C., Jin, X., Wong, K. C., Shi, M., & Lio, P. (2012). Collective human mobility pattern from taxi trips in Urban Area. *PloS One, 7*(4), e34487.
Rhee, I., Shin, M., Hong, S., Lee, K., Kim, S. J., & Chong, S. (2011). On the levy-walk nature of human mobility. *IEEE/ACM Transactions on Networking (TON), 19*, 630–643.
Roth, C., Kang, S. M., Batty, M., & Barthelemy, M. (2011). Structure of urban movements: Polycentric activity and entangled hierarchical flows. *PloS One, 6*(1), e15923.
Sobel, A. H., & Tippett, M. K. (2018). *Extreme events: Trends and risk assessment methodologies. Resilience*. Elsevier3–12.
Song, C., Qu, Z., Blumm, N., & Barabási, A. L. (2010). Limits of predictability in human mobility. *Science, 327*, 1018–1021.
Tang, J., Liu, F., Wang, Y., & Wang, H. (2015). Uncovering urban human mobility from large scale taxi GPS data. *Physica A, 438*, 140–153.
Van Aalst, M. K. (2006). The impacts of climate change on the risk of natural disasters. *Disasters, 30*, 5–18.
Wang, M., Huang, L., & Yan, X. (2012). Exploring the mobility patterns of public transport passengers. *Journal of University of Electronic Science and Technology of China, 41*(1), 2–7.
Wang, M., Yang, S., Sun, Y., & Gao, J. (2017). Human mobility prediction from region functions with taxi trajectories. *PloS One, 12*(11), e0188735.
Wang, M., Yang, S., Sun, Y., & Gao, J. (2017). Human mobility prediction from region functions with taxi trajectories. *PloS One, 12*(11), e0188735.
Wang, Q., & Taylor, J. E. (2014). Quantifying human mobility perturbation and resilience in hurricane sandy. *PloS One, 9*, e112608.
Wang, Q., & Taylor, J. E. (2016). Patterns and limitations of urban human mobility resilience under the influence of multiple types of natural disaster. *PloS One, 11*, e0147299.
Wang, W., Pan, L., Yuan, N., Zhang, S., & Liu, D. (2015). A comparative analysis of intra-city human mobility by taxi. *Physica a-Statistical Mechanics and Its Applications, 420*, 134–147.
Wang, Y. (2017). *Three flights were canceled and 75 flights were delayed in Nanjing due to rainstorm.* Accessed 12 November 2018:http://news.jschina.com.cn/focus/201706/t20170610_629743.shtml.
Wang, Y., & Taylor, J. E. (2018). Coupling sentiment and human mobility in natural disasters: A Twitter-based study of the 2014 South Napa Earthquake. *Natural Hazards, 92*, 907–925.
Wang, Y., & Taylor, J. E. (2017). Tracking urban resilience to disasters: A mobility network-based approach. *Proceedings of 14th ISCRAM Conference,* 97–109.
Wang, Y., Wang, Q., & Taylor, J. E. (2017). Aggregated responses of human mobility to severe winter storms: An empirical study. *PloS One, 12*, e0188734.
Yabe, T., Tsubouchi, K., Sudo, A., & Sekimoto, Y. (2016). *A framework for evacuation hotspot detection after large scale disasters using location data from smartphones: Case study of Kumamoto earthquake. Proceedings of ACM Sigspatial International Conference on Advances in Geographic Information Systems*44.
Yang, Y., Ng, S. T., Zhou, S., Xu, F. J., & Li, H. (2019). A physics-based framework for analyzing the resilience of interdependent civil infrastructure systems: A climatic extreme event case in Hong Kong. *Sustainable Cities and Society, 47*, 101485.
Yao, C. Z., & Lin, J. N. (2016). A study of human mobility behavior dynamics: A perspective of a single vehicle with taxi. *Transportation Research Part A: Policy and Practice, 87*, 51–58.
Yin, J., Yu, D., Lin, N., & Wilby, R. L. (2017). Evaluating the cascading impacts of sea level rise and coastal flooding on emergency response spatial accessibility in Lower Manhattan, New York City. *Journal of Hydrology, 555*, 648–658.
Yuan, J., Zheng, Y., & Xie, X. (2012). Discovering regions of different functions in a city using human mobility and POIs. *Proceedings of the 18th ACM SIGKDD International Conference on Knowledge Discovery and Data Mining,* 186–194.
Zanni, A. M., & Ryley, T. J. (2015). The impact of extreme weather conditions on long distance travel behaviour. *Transportation Research Part A: Policy and Practice, 77*, 305–319.
Zheng, Z., Rasouli, S., & Timmermans, H. (2016). Two-regime pattern in human mobility: Evidence from GPS taxi trajectory data. *Geographical Analysis, 48*, 157–175.